Sparse Operation of Multi-Winding Transformer in Multiport-Ac-Coupled Converters

Youssef Elasser, Yenan Chen, Ping Wang, Minjie Chen
Princeton University, Princeton, NJ, United States
Email: {yelasser, yenanc, pwang2, minjie}@princeton.edu

***Abstract*—The multi-winding transformer in a Multiport-Ac-Coupled (MAC) converter interfaces with a large number of ac-dc ports and processes multi-way power flow. This paper investigates the *"sparse operation"* of multi-winding transformers, i.e. *when only a few windings deliver power and a majority of the windings remain open-circuited*. These open-circuited windings induce additional leakage inductance and skin & proximity effects in planar magnetics, change the circuit behavior, and increase the losses. By modeling a ten-winding PCB-embeded planar transformer in SPICE, the impact of "sparse operation" on transformer performance is predicted. To verify the theoretical modeling and simulation results, the performance of a 10-winding planar PCB transformer is experimentally compared to the performance of a 10-winding litz wire transformer in a 10-port MAC converter while transferring power from one winding to another. In the planar transformer, it is observed that windings that are physically closer to each other can transfer more power at higher efficiencies than those that are further, while this trend is not present in the litz wire transformer.**

***Index Terms*—sparse operation, multiwinding transformer, planar magnetics, multi-active-bridge converter.**

I. Introduction

Power converter topologies that can interface with multiple sources and loads are needed in a wide range of power electronics systems. Many applications such as data centers, solar farms, and battery storage systems consist of numerous modules that need multiport power management. Fig. 1 illustrates two example applications where multiport power converters are used, one for battery management systems (BMS), and one for solar maximum power point tracking (MPPT). A traditional way of processing and delivering multi-way power flow is to create a dc voltage bus to which each "dc-dc" unit can transfer power. While this allows for simple control of each individual module, this comes at the expense of multiple conversion stages to transfer power between two ports. A "dc-ac-dc" process transfers power from one port to the dc bus, and another "dc-ac-dc" process is needed to transfer power from the bus to the other port.

The Multiport-Ac-Coupled (MAC) architecture, shown in Fig. 2, mitigates this issue by reducing the number of power conversion stages. By coupling multiple "dc-ac" ports via a multi-winding transformer, power being transferred now only needs to go through a single "dc-ac-dc" stage. Another benefit of this solution is that the magnetic core area can be significantly reduced, as all windings will have an identical volt-seconds-per-turn [1].

978-1-7281-1842-0/19/$31.00 ©2019 IEEE

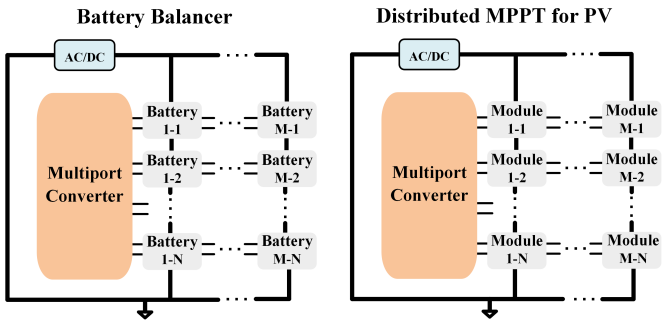

Fig. 1. A multiport converter configured as a 1) battery balancer for grid scale energy storage and 2) distributed MPPT for photovoltaic systems. Energy is delivered from one port to another through the multiport converter.

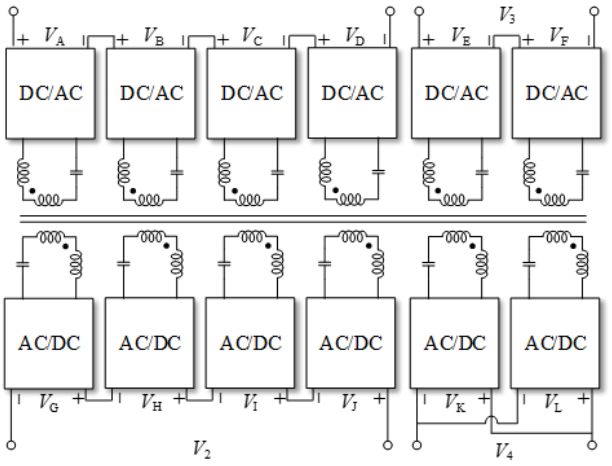

Fig. 2. A MAC converter implemented with many dc-ac and ac-dc modules and a single magnetic core. Multiple "dc-ac" modules can be connected in series or parallel to synthesize input/output ports for a range of voltage and current ratings. The MAC converter can be implemented as a Multi-Active-Bridge (MAB) converter or a Multiport-Series-Resonant (MSR) Converter [1].

Many applications, such as energy routers, electric vehicles, and high-power electronic traction systems have adopted the MAC architecture for managing power distribution [2]–[4]. Furthermore, multiple-output converters, such as that presented in [5] for satellite applications, use multi-winding transformers to AC couple multiple outputs to one input port. The multi-winding transformer is typically implemented with a planar magnetic structure with printed-circuit-board (PCB) windings in order to improve the efficiency and the power density of the isolation stage [6], [7].

While ac-coupling of multiple ports comes with the advantage of reduced power conversion stress, this approach is not without its drawbacks. One of the major challenges in MAC converters is that as the number of ports increases, the power flow becomes increasingly sophisticated [8]. Particularly for applications consisting of many modular units, the multi-winding transformer will typically operate without all of the windings being active. Many of the windings will be effectively open-circuited or carry very low current. This phenomenon, termed *"sparse operation,"* impacts the design of the multi-winding transformer.

This paper investigates the impact of "sparse operation" on multi-winding transformers through theoretical analysis, numerical simulation, and experimental measurements. Modeling techniques for multi-winding transformers are employed to develop a circuit model that can be easily simulated in SPICE. Various design parameters such as number of ports, switching frequency, and geometry are analyzed. Finite element analysis is used to further verify the effectiveness of the model in analyzing sparse operation. A prototype of a MAC converter is built with a planar magnetic structure and PCB windings and compared against a similar converter with a twisted litz wire based transformer to observe how sparse operation impacts the different structures.

II. Sparse Operation of Multi-Winding Transformers

There are various ways of controlling the multi-input multi-output (MIMO) power flow in a MAC converter. As discussed in [8], two techniques that can be used to control the power flow are phase-shift control and time-sharing control. While phase-shift control reduces the voltage and current stress on devices as well as the energy storage requirements, the power flow is cross coupled and very complicated. Time-sharing control, on the other hand, only activates two ports at a time, deactivating the other ports. This greatly simplifies the power flow control of a multiport system, especially in light load conditions. For a MAC converter operated with time-sharing control, a majority of the windings are "open-circuited" and the winding stacks are highly sparse.

Fig. 3 shows the principles of this control scheme. During a time sharing period T_s, power is delivered from port 1 to port 2 during D_2T_s, from port 1 to port 3 during D_3T_s, and from port 1 to port 4 during D_4T_s. During D_2T_s, only the windings connected to port 1 and port 2 are active, while the windings connected to port 3 and 4 are not active. This discontinuous operation of the multi-winding transformer will make the converter operate in sparse mode. As the number of ports scales up, an increasing amount of ports are left open-circuited.

III. SPICE Models for Multi-Winding Planar Transformer

To investigate the sparse operation of a multi-winding planar transformer, the modular layer model (MLM) presented in [6] is adopted. Fig. 4 shows a multi-winding planar transformer with an arbitrary number of dc-ac ports. In this model, each

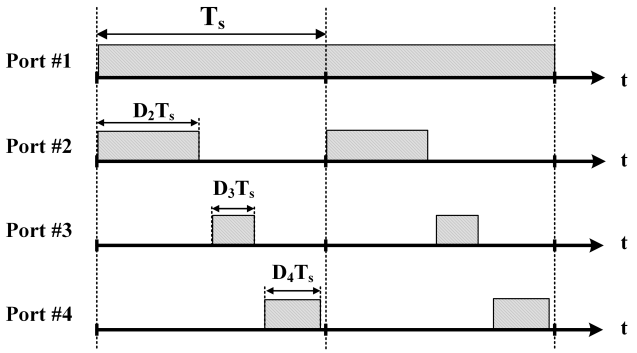

Fig. 3. A four port multiport converter operating under time sharing control, where port 1 is the input and ports 2, 3, and 4 are the output.

one of these layers can be considered as a modular unit and a lumped circuit model can be created that is comprised of multiple modular circuit blocks. Each sub-circuit block represents a portion of the magnetic structure. The magnetic reluctance on top and bottom of the layer stack, the conductor layers, and the spacings are all captured within this model. Under 1-D and magnetoquasistatic (MQS) assumptions, this model can also analytically capture skin and proximity effects in the windings. In this work, we use the MLM model to explain and investigate the sparse operation of multi-winding planar transformer.

A step-by-step procedure is used to generate a lumped circuit model of the multi-winding transformer. Each conductor layer i is modeled as a three-terminal impedance network as illustrated in Fig. 5. The "horizontal" impedances $\frac{d_i}{w_i}Z_{ai}$ and the "vertical" impedance $\frac{d_i}{w_i}Z_{bi}$, where d_i and w_i are the length and width of layer i, are determined according to

$$\begin{aligned} Z_{ai} &= \frac{\Psi_i \left(1 - e^{-\Psi_i h_i}\right)}{\sigma_i \left(1 + e^{-\Psi_i h_i}\right)}, \\ Z_{bi} &= \frac{2\Psi_i e^{-\Psi_i h_i}}{\sigma_i \left(1 - e^{-\Psi_i h_i}\right)}, \\ \Psi_i &= \frac{1+j}{\delta_i}, \\ \delta_i &= \sqrt{\frac{2}{\omega \mu_i \sigma_i}}, \end{aligned} \tag{1}$$

Here ω is the operating angular frequency, μ_i and σ_i are the permeability and conductivity, respectively, of the conductive material, and h_i is the layer thickness. δ_i represents the skin depth of the conductor. All layers can be approximated to have the same length $d_i = d$ and width $w_i = w$ under the 1-D assumption.

In order to capture the effect of the spacings between adjacent layers, additional impedances are added between layers. Given the spacing between layer i and layer $i+1$ with thickness a_i, an impedance of $\frac{d}{w}Z_{Si}$ can be placed in between these two layers, where

$$Z_{Si} = j\omega\mu_i a_i \tag{2}$$

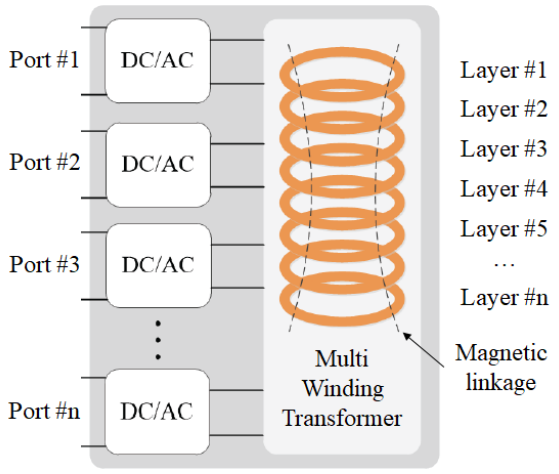

Fig. 4. A multi-winding transformer with n dc-ac ports.

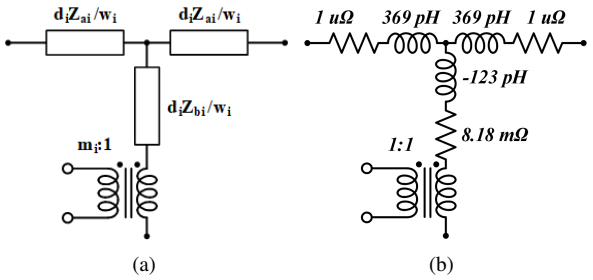

Fig. 5. (a) Three-terminal network of a singular conductor layer. (b) Lumped circuit model of the 100-layer example structure under investigation.

The effect of the magnetic core, as well as any air gaps, are modeled by impedances on both sides of the circuit. The impedance representing the top and bottom of the magnetic core is Z_T and Z_B, where

$$\begin{aligned} Z_T &= j\omega/\mathcal{R}_T \\ Z_B &= j\omega/\mathcal{R}_B \end{aligned} \tag{3}$$

$\mathcal{R}_T$ and $\mathcal{R}_B$ represent the magnetic reluctances of the top and bottom of the core, respectively. Adding additional shunt resistances captures the impacts of core loss.

The full lumped circuit model of an n layer multi-winding transformer is shown in Fig. 6. L_{MT} and L_{MB} represent the magnetizing energy stored in the core. R_{MT} and R_{MB} capture the core loss. L_T, L_B, and L_G represent the energy stored in each conductive layer. L_S represents the energy storage in the spacings between adjacent winding layers (leakage inductance). R_T, R_B, and R_G capture the power loss in the windings considering skin and proximity effects. The turns ratio of the ideal transformers in each layer is determined by the number of turns in each layer.

By analyzing and simulating this lumped circuit model with the external driving circuits and probing the current flowing through the corresponding subcircuits in the SPICE simulation, the current flowing through each layer can be visualized and evaluated in SPICE.

Based on the MLM model, we make the following two hypothesises for multi-winding planar magnetics operated in "sparse operation":

- The spacings between two active windings induce additional impedance between the two active ports. With the same external exciation (voltage source or current source), this impedance will set the maximum power that can be transferred between two ports with a given excitation. Less power can be transferred between ports that are physically further away (with lots of "open" windings in the middle).
- The propagation of the electromagnetic field between two "active" windings will induce eddy current in the "open windings" due to skin and proximity effects. The eddy current will induce additional loss in the "open windings" and will have an impact on the system efficiency.

IV. SPICE Simulation of Planar Magnetics in Sparse Operation

To observe the effects of sparse operation on power transfer between two layers of a MAC converter, SPICE simulation is used. Using the M2SPICE netlist generation tool, information about the geometry of a planar PCB transformer is provided as an input and a SPICE netlist is generated [9]. A simulation testbench of a 100-layer multi-winding transformer is created to observe the impact of a high percentage of open circuited ports. A ten-layer multi-winding transformer is also simulated and later experimentally verified.

A. 100-Layer Multi-Winding Transformer Simulation

Fig. 5b shows the MLM of a single layer in the 100-layer multi-winding transformer model. For this simulation, all of the spacings between the layers were set at 1.2 mm. This induces a leakage inductance L_s of 25.53 μH. The height of each layer is 34.7 μm and the width is 2.54 mm. The winding length per layer is 4.2 cm. The effective core area is 59 mm^2, and the relative permeability μ_r of the core is 1430. The switching frequency f_s is 100 kHz. Each winding consists of 1 turn. The magnetizing inductances L_{MT} and L_{MB} are both 89 μH. The core loss resistances R_{MT} and R_{MB} are both 7.6 Ω.

The 100-layer multi-winding transformer model is connected to a dual-active-bridge (DAB) simulation platform in PLECS. The on-resistance $R_{ds_{on}}$ of each of the four MOSFETs is 3 mΩ. The dc-blocking capacitance value is 300 μF. The input source and output load voltages are both 5V. To modulate the power transferred, the phase shift between the two half-bridges is adjusted. Layer #1 is set as the input port, and the output is swept from layer #10 to layer #100 in intervals of 10. The dc-dc converter efficiency at various output powers for each of the scenarios is recorded.

Fig. 7 shows the dc-dc converter efficiency results against the output power of the DAB converter for 6 different cases: power transfer from layer #1 to layers #10, #20, #30, #40, #70, and #100.

Two observations are made from these simulation results with the DAB simulation platform:

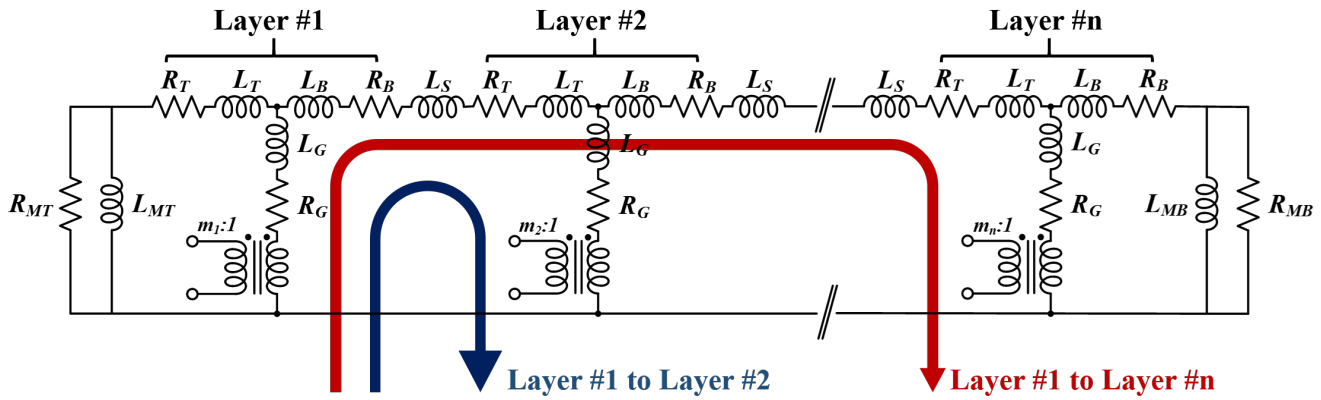

Fig. 6. Modular layer model of an n layer multi-winding transformer. Transferring power from layer #1 to layer #2 and transferring power from layer #1 to layer #n induces different losses.

TABLE I
MAXIMUM TRANSFERRABLE POWER IN A 100-LAYER MULTI-WINDING TRANSFORMER: SIMULATION RESULTS

1→10	1→20	1→30	1→40	1→70	1→100
10.38W	7.53W	5.80W	4.67W	2.78W	1.85W

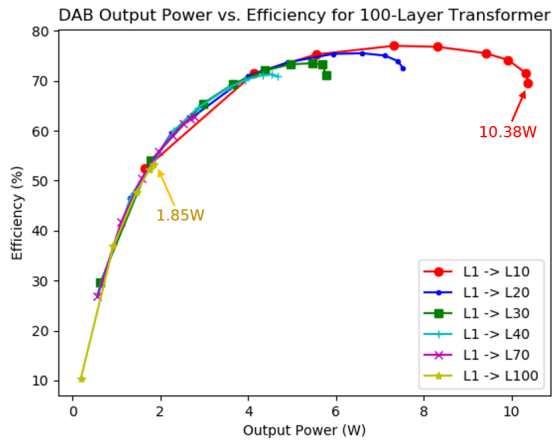

Fig. 7. 100-port DAB converter efficiency vs. output power when transferring power from layer #1 to layers #10, #20, #30, #40, #70, and #100.

1) As the physical distance away from the input layer increases, the amount of power that can be transferred decreases. Table I lists the maximum power that can be transferred from layer #1 to the other layers. A sharp decrease from layer #10 to layer #100 is seen. This means that, according to the MLM, the amount of power that can be transferred from one layer to another is a function of the physical distance between the two layers.
2) At higher output powers, the efficiency of power transfer from one layer to another is higher when the layers are closer to each other during sparse operation. As the physical distance between two layers increases, more reactive power is needed to transfer the same real power from port to port. The efficiency will also decrease due to the additional loss in the "open" layers.

B. Ten-Layer Multi-Winding Transformer Simulation

While the 100-port simulation gives insight into the mechanism of sparse operation of a multi-winding transformer, a transformer of this geometry would be unpractical to build. To implement a design example that can be experimentally verified, a ten-layer multi-winding transformer geometry was also provided as an input to M2SPICE. The single layer MLM is the same as that of Fig. 5b. The layer height, thickness, and width remain the same as well. The only change is in the spacing between the layers. From top to bottom, the thicknesses of the nine spacings between the ten layers are $\{0.12, 1.2, 0.12, 0.07, 0.12, 1.2, 0.12, 0.07, 0.12\}$ mm, respectively. The geometry is asymmetrical with uneven spacing between layers. The leakage inductances that were induced by the nine spacings between the ten layers are $\{2.55, 25.53, 2.55, 1.49, 2.55, 25.53, 2.55, 1.49, 2.55\}$ μH from top to bottom respectively. Fig. 8 shows the complete SPICE model of the multi-winding transformer.

The same simulation conducted for the 100-layer transformer was done for the ten-layer case. Fig. 9 shows the multi-winding transformer configured in a DAB setup in PLECS. Fig. 10 shows the dc-dc converter efficiency against the output power for power transfer from layer #1 to layers #2, #5, and #10. The same trend as with the 100-layer simulation is observed. In this scenario, there is only a 2 Watt difference between the maximum power transferred between layer #1 and layer #2 vs. layer #1 and layer #10.

The MLM thus provides useful insights into how many layers a multi-winding transformer for an MAC converter should have. By simply knowing the geometry information of the proposed design, the MLM approach can rapidly generate a SPICE netlist of this transformer that can be used in SPICE simulation. These simulations are much less computationally intensive than a finite element analysis, and can capture the skin and proximity effects which can not be rapidly captured by other analytical models. The experimental results show that while a planar transformer is suitable for a ten-layer multi-winding design for this geometry, scaling up to beyond 30 layers will present challenges when the converter is in sparse operation. The layer thickness and spacing can be jointly optimized to extend the power delivery range.

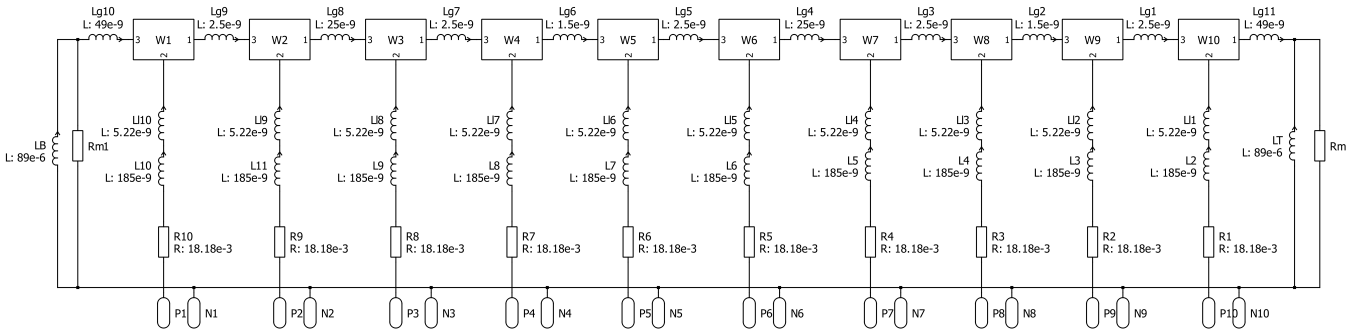

Fig. 8. SPICE model of the ten-layer planar transformer with ten modular layer building blocks of Fig. 5b W1-W10.

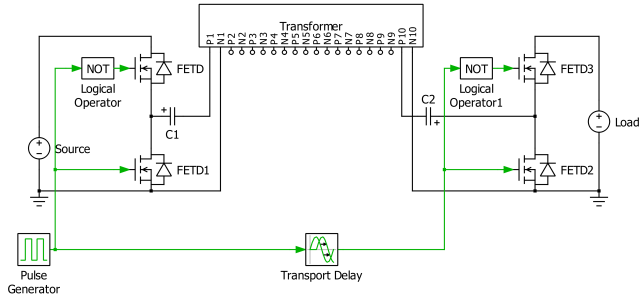

Fig. 9. A ten-layer multi-winding transformer in a MAC dual-active-bridge converter in PLECS.

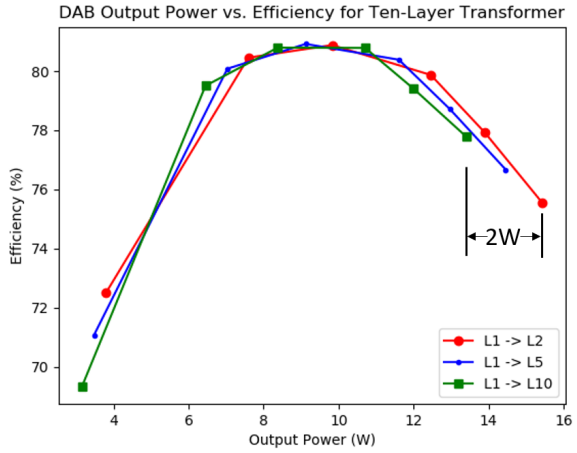

Fig. 10. Ten-port DAB converter efficiency vs. output power when transferring power from layer #1 to layers #2, #5, and #10.

V. Finite Element Analysis

To further investigate the trend of decreasing efficiency as the distance between layers increases in a planar transformer, a finite element model is built in ANSYS Maxwell 3-D simulation platform. The geometry of the ten-layer multi-winding transformer detailed in Section IV-B is used. A current excitation pointing into layer #1 represents the input power, and a current excitation pointing out of the other layers is used to represent the output power. Simulations are conducted using layer #1 as the input and layer #2 or layer #10 as the output. The other windings are open-circuited by

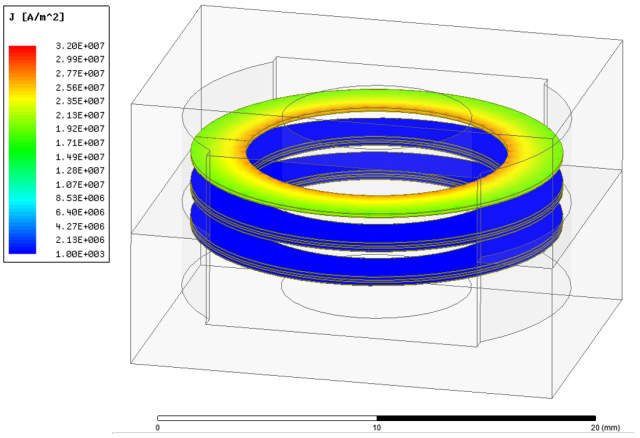

Fig. 11. 3-D FEM simulation of a planar PCB transformer. Power is transferred from layer #1 to layer #2 at 100 kHz.

physically disconnecting the conductor layers. Eddy current along the radial and axial directions can still be excited by the skin and proximity effects.

Simulations are conducted at frequencies of 25 kHz, 100 kHz, and 1 MHz. Fig. 11 shows the results of the 100 kHz simulation when layer #2 is set as the output. The current density in the "open" windings transferring power from layer #1 to layer #2 is negligible (e.g., layer #3-#10). This represents a negligible amount of eddy current induced in the "open" layers when power is being transferred between layers that are physically close. The finite element analysis at 25 kHz and at 1 MHz displays similar results as the 100 kHz analysis when transferring power to layer #2.

Fig. 12 shows the results of the 25 kHz (top), 100 kHz (middle), and 1 MHz (bottom) simulations when transferring power from layer #1 to layer #10. The other "open" windings have a non-negligible current density, which leads to increased copper loss due to skin and proximity effects. This effect becomes more prominent as frequency increases. In the 1 MHz simulation, windings 7, 8, and 9 have eddy currents that are comparable in magnitude to that of the windings that are transferring or receiving power. This matches with the insights developed from the SPICE simulations of the MLM. Layers that are further apart from each other will incur more losses when transferring the same amount of power as those that are closer to each other.

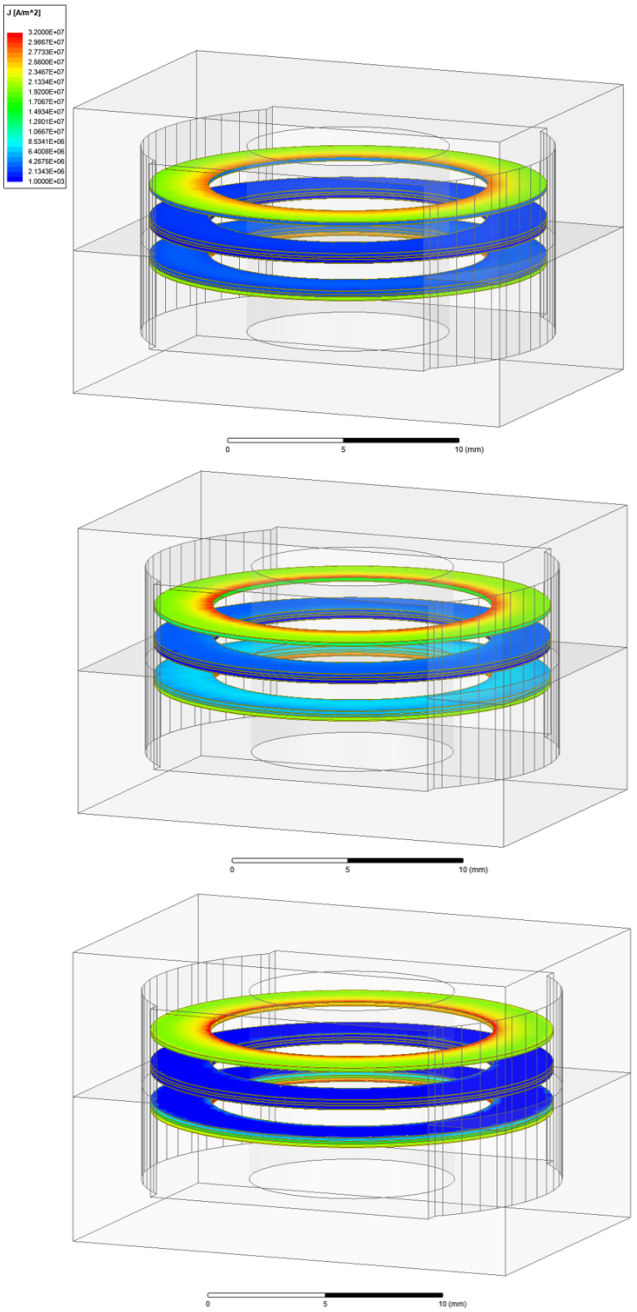

Fig. 12. 3-D FEM simulation of a planar PCB transformer. Power is transferred from layer #1 to layer #10 at 25 kHz (top), 100 kHz (middle), and 1 MHz (bottom).

VI. Experimental Results

A prototype of a ten-port MAC multi-active-bridge converter is designed and implemented to experimentally verify the simulation results. Fig. 13 shows the prototypes of the converter with two different transformers as well as the cross-sections of the transformers. One is constructed with a ten-layer PCB planar transformer with the same geometry presented in Section IV-B. The other converter is ac-coupled with a ten-winding twisted litz wire transformer. The performance of the twisted litz wire transformer is also impacted by the sparse operation. However, since the litz wires are twisted, no clear performance trend from winding to winding should be observed. Table II lists the specifications of the converter.

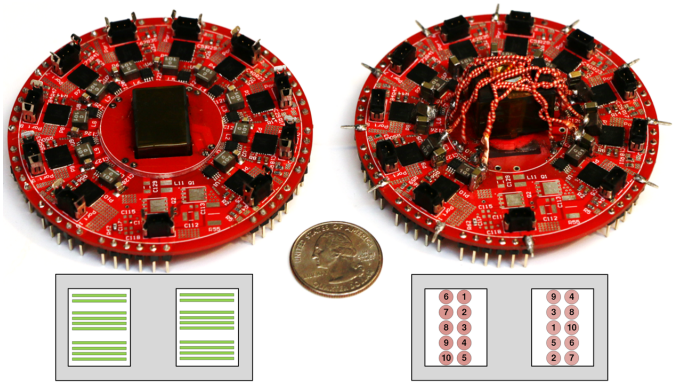

Fig. 13. Prototype and front-facing cross section of a 10-port MAC converter with a PCB planar transformer (left) and a twisted litz wire transformer (right). The schematic of the MAC converter is shown in Fig. 2.

TABLE II
Specifications of the MAC Converter

Specifications & Symbol	Description
Rated Port Power: $P_1 - P_{10}$	30W
Rated Port Voltage: $V_1 - V_{10}$	5V
Size	Height: 1.2 cm Radius: 3.7 cm
Power Density	100 W/in^3
Port #1–#10 Switches	ON Semiconductor FDMF6833C DrMOS, 50A
Transformer Core	TDK EEQ20-N97, $\mu_r = 1430$
Inductors: $L_{ext,1} - L_{ext,10}$	100nH
Capacitors: $C_{b1} - C_{b10}$	141μF

To test how the efficiency changes as a function of layer distance for the planar transformer, the input port was set to be the port connected to the top layer winding. Power was then transferred from this port to all other ports on the board. To mimic sparse operation, the other windings were left open while power was being transferred from the input to the output port. Experiments were conducted at switching frequencies of 100 kHz and 200 kHz. The output power was swept by modulating the phase shift between the two half-bridges, as done in Sections IV-A and IV-B.

Both observations made in Section IV-A should be observable in this experiment. The maximum transferrable power should be less when transferring power from layer #1 to layer #10 when compared to layer #1 to layer #2. In addition, the skin and proximity effects in the windings should induce eddy current loss in the open-circuited layers, as seen in the simulations. This will be reflected in the measured dc-dc efficiency from port to port.

Fig. 14 shows a plot of the dc-dc port-to-port converter efficiency against the output power for a switching frequency of 100 kHz. Just as in Fig. 10, plots of power transfer from layer #1 to layers #2, #5, and #10 are shown. The maximum transferrable power from layer #1 to layer #2 is 13.51 W, and

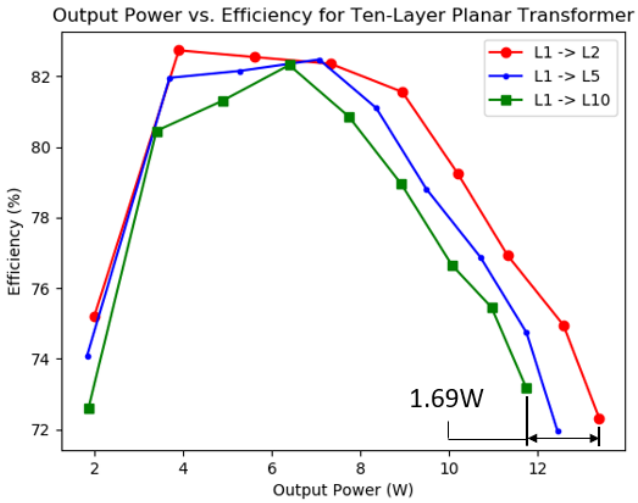

Fig. 14. Experimental efficiency results of the MAC converter with a ten-port planar transformer vs. output power when transferring power from layer #1 to layers #2, #5, and #10 at 100 kHz switching frequency.

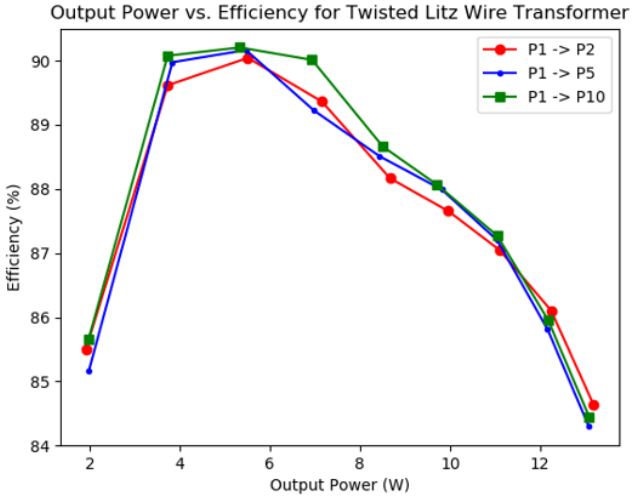

Fig. 16. Experimental efficiency results of the MAC converter with a ten-port twisted litz wire transformer vs. output power when transferring power from layer #1 to layers #2, #5, and #10 at 100 kHz switching frequency.

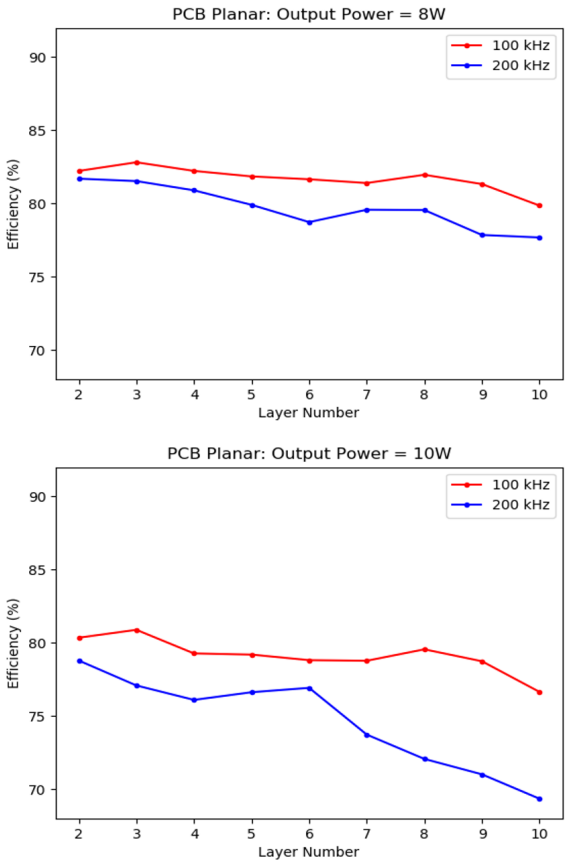

Fig. 15. Measured efficiency of power transfer from layer #1 to all other layers for the planar transformer MAC converter at 8 W and 10 W.

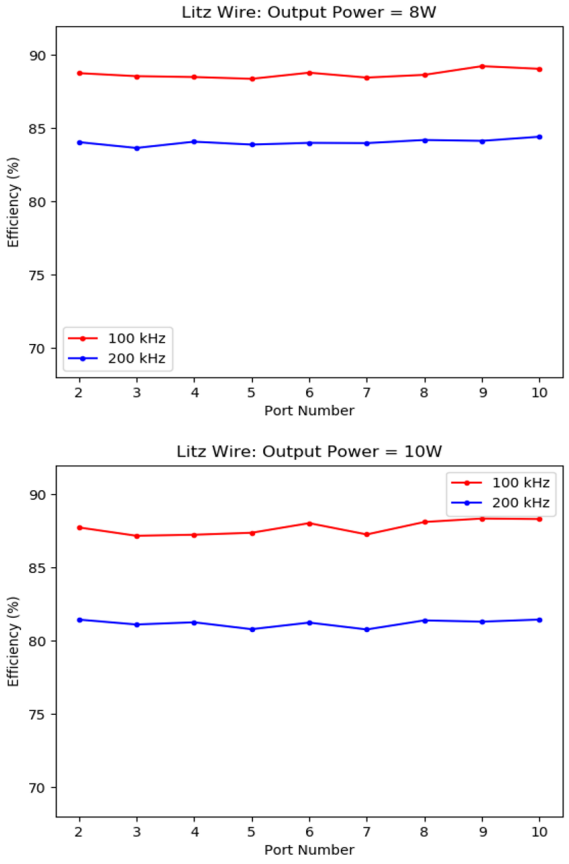

Fig. 17. Measured efficiency of power transfer from layer #1 to all other layers for the twisted litz wire transformer MAC converter at 8 W and 10 W.

the maximum transferrable power from layer #1 to layer #10 is 11.82 W. This difference of 1.69 W is comparable to the 2 W difference observed in the simulation in IV-B. In simulation, the maximum transferrable power from layer #1 to layer #2 is 15.44 W, and the maximum transferrable power from layer #1 to layer #10 is 13.41 W. This discrepancy of around 2 W is due to lack of modeling of trace resistances such as the ESR of the inductors and capacitors, as well as not including the output capacitance C_{oss} of the MOSFET switches.

Fig. 15 shows the dc-dc converter efficiency plotted against the layer number that power was being transferred to. This was done at two output powers: 8W and 10W. For both the

100 kHz case as well as the 200 kHz case, the efficiency drops as the physical distance from layer #1 increases. This effect is most prominently seen at a switching frequency of 200 kHz with an output power of 10W. For further away layers, 10W is close to the maximum transferrable power threshold. This is more pronounced at 200 kHz due to the increased AC winding resistance as a result of increased skin and proximity effects.

The same experimental setup is used for the MAC converter with the twisted litz wire transformer. Since the litz wires are twisted, and the ten-port system is more symmetric, the efficiency from one port to another should remain relatively constant when transferring power from port #1 to other ports. In addition, the maximum transferrable power should not be a function of the ports that are transferring power.

Fig. 16 plots the dc-dc port-to-port converter efficiency against the output power. Unlike in the planar PCB transformer, these curves overlap. With the twisted litz wire transformer, transferring power from one port to any other port results in a similar efficiency-output power curve.

Fig. 17 shows the dc-dc converter efficiency plotted against the port number, where port #1 is held constant as the input power port and the output power port was swept from port #2 to port #10. Whereas a noticeable trend of declining efficiency as the layer distance increased is noticed in the planar transformer converter, no such trend is observed with the litz wire transformer. The efficiency remains relatively constant for all ports, confirming the initial hypothesis that this transformer would not be subject to the same effects as the planar transformer during sparse operation.

VII. Design Guidelines for Sparse Operation

Sparse operation of multi-winding transformers should be carefully considered when designing these transformers for MAC converters. As the number of ports in an MAC converter increases, ports that are connected to "far-away" transformer windings can not transfer as much power as ports that are closer. A sharp decrease in the maximum possible power transfer is observed above 20 ports for the transformer geometry presented in this paper. Using M2SPICE to generate a netlist of a proposed design allows for quick simulation to see what the port threshold is.

Experimental results confirmed that for a ten-port MAC converter, a litz wire transformer offered some advantages over a planar transformer. However, for this system, either multi-winding transformer would suffice under sparse operation. The tradeoff of lower modularity and repeatability that exist with litz wire transformer means that for a lower port count design, it is typically preferable to use a planar design. The performance of a twisted litz wire transformer in sparse operation also highly depends on how well the litz wires are twisted [10]. At MHz frequencies, litz wire is no longer attractive as the strands are usually not thin enough [11].

The switching frequency of the system also has a high impact on a planar transformer operating in sparse operation. Increasing the switching frequency allows for a reduction of the size of the magnetic components. High switching frequencies result in high eddy currents in open circuited windings when the converter is in sparse operation. If the converter operates in sparse operation often, reducing the switching frequency can offer performance benefits. This was observed in the prototype experiments. Compared to 100 kHz, operating at 200 kHz resulted in worse converter efficiency as well as a sharper dropoff in the maximum transferrable power between closer layers and farther layers.

VIII. Conclusion

This paper presents the analysis and design of a multi-winding transformer in multiport ac-coupled converters with "sparse operation," where only a few windings carry significant current and a majority of windings remain open-circuited during operation. These open-circuited windings suffer from skin and proximity effect and contribute additional losses. A planar PCB transformer and a twisted litz wire transformer is designed, analyzed, and implemented for a 10-port multi-active-bridge converter. It is observed that the planar PCB transformer's port-to-port power conversion efficiency is a function of which layer the winding is with respect to the layer of the port transferring power. For the twisted litz wire transformer, the port-to-port efficiency is independent of the ports that are activated (due to port-to-port symmetry).

References

[1] P. Wang and M. Chen, "Towards Power FPGA: Architecture, Modeling and Control of Multiport Power Converters," *IEEE 19th Workshop on Control and Modeling for Power Electronics (COMPEL)*, Padova, 2018, pp. 1-8.

[2] X. Liu, Z. Zheng, K. Wang and Y. Li, "An energy router based on multi-winding high-frequency transformer," *2016 IEEE Applied Power Electronics Conference and Exposition (APEC)*, Long Beach, CA, 2016, pp. 3317-3321.

[3] J. Schfer, D. Bortis and J. W. Kolar, "Multi-port multi-cell dc/dc converter topology for electric vehicle's power distribution networks," *2017 IEEE 18th Workshop on Control and Modeling for Power Electronics (COMPEL)*, Stanford, CA, 2017, pp. 1-9.

[4] C. Gu, Z. Zheng, L. Xu, K. Wang, and Y. Li, "Modeling and Control of a Multipower Electronic Transformer (PET) for Electric Traction Applications," *IEEE Transactions on Power Electronics*, vol. 31, no. 2, pp. 915-927, Feb. 2016.

[5] D. Hu, D. Ye, Z. Zhang, B. He, and X. Ren, "Optimal Design of Multi-Winding Planar Transformers in 1 MHz GaN Multiple-Output Forward Converters," *2018 IEEE Applied Power Electronics Conference and Exposition (APEC)*, San Antonio, TX, 2018, pp. 2288-2293.

[6] M. Chen, M. Araghchini, K. K. Afridi, J. H. Lang, C. R. Sullivan and D. J. Perreault, "A Systematic Approach to Modeling Impedances and Current Distribution in Planar Magnetics," *IEEE Transactions on Power Electronics*, vol. 31, no. 1, pp. 560-580, Jan. 2016.

[7] M. Chen, K. K. Afridi, S. Chakraborty and D. J. Perreault, "Multitrack Power Conversion Architecture," in *IEEE Transactions on Power Electronics*, vol. 32, no. 1, pp. 325-340, Jan. 2017.

[8] Y. Chen, P. Wang, H. Li, and M. Chen, "Power Flow Control in Multi-Active-Bridge Converters: Theories and Applications," *IEEE Applied Power Electronics Conference and Exposition (APEC)*, Los Angeles, March 2019.

[9] S. Gunter, M. Chen, S. A. Pavlick, R. Abranson, K. K. Afridi, and D. J. Perreault, "Applicability and Limitations of a M2Spice-assisted Time-Domain Current Calculation and Visualization Approach for Planar Magnetics," *IEEE Applied Power Electronics Conference and Exposition (APEC)*, Long Beach, CA, March, 2016.

[10] C. R. Sullivan, "Analytical model for effects of twisting on litz-wire losses," *IEEE Workshop on Control and Modeling for Power Electronics (COMPEL)*, Santander, 2014, pp. 1-10.

[11] B. A. Reese and C. R. Sullivan, "Litz wire in the MHz range: Modeling and improved designs," *IEEE Workshop on Control and Modeling for Power Electronics (COMPEL)*, Stanford, CA, 2017, pp. 1-8.